Computational And Biological Studies Of Platinum(II) Complex Of Tryptathrin Schiff Base

Milan P. Dhaduk
Sardar Patel University
Ravi A. Dabhi
Sardar Patel University
Bhupesh S. Bhatt
Sardar Patel University
Vaibhav D. Bhatt
Gujarat Technological University
Mohan N. Patel (jeenen@gmail.com)
Sardar Patel University https://orcid.org/0000-0001-9016-9245

Research Article

Keywords: Pt(II) complexes, DNA binding, Antimicrobial activity, Anticancer activity, DFT

Posted Date: May 6th, 2022

DOI: https://doi.org/10.21203/rs.3.rs-1605334/v1

Abstract

A series of tryptanthrin alkaloid based ligands (L^1-L^7) and corresponding platinum(II) complexes were synthesized and characterized by various spectroscopic techniques, LC-MS, magnetic measurement, and electronic spectra. DFT studies were performed for structure optimization. Viscosity measurement, UV-Vis spectroscopy, and molecular docking studies were used to determine the binding mode between CT-DNA and complexes; the intercalation mode of bindings was concluded from the study. The K_b values for compounds-DNA binding were found in the range of $0.42 \times 10^5 – 3.90 \times 10^5$ M^{-1}. The binding study of complexes with BSA was evaluated by fluorescence quenching study, and the value of Ksv, binding constant (Ka), and binding site(n) were in the range of $1.14–2.70 \times 10^3$ M^{-1}, $0.13–0.55 \times 10^5$ M^{-1}, and 0.94–1.16, respectively. Bacteriostatic activity of the synthesized compound was performed against gram + ve and gram -ve bacteria. MIC values of complexes and ligands were found in the range of 35–75 μM and 150–245 μM, respectively. BSLB was performed to check the cytotoxicity of the synthesized compounds. The LC_{50} values of the ligands and complexes were found in the range of 9.24–11.18 μg/mL and 5.9–7.94 μg/mL, respectively. Anticancer activity against the MG-63 cell line was performed to check potency against the cancer cell line. The IC_{50} values of the synthesized compounds were found in the range of 10.9 μg/mL 28.7μg/mL. IC_{50} value of the complex III is 10.9 μg/mL, which is comparable with the standard drug cisplatin.

Introduction

The polynuclear N-heterocyclic compounds with fused multi-ring skeletons are not just of significant interest to the medication and colour industry but also crucial in organic synthesis [1–3]. Among the different N-heterocycles, quinazoline-4(3H)-one fused polycyclic systems are especially inferable from their pervasiveness in a couple of natural products, for example, Luotonin A, Rutaecarpine, Tryptanthrin, Cephalanthrin A, Phaitanthrin, and Cruciferae. On the other hand, indolo[2,1-b] quinazoline-6,12-dione, is a fascinating theme because of its rife structural features[4]. However, regardless of the motivating property, a synthetic route for tryptanthrin (unsubstituted indolo[2,1-b]quinazoline-6,12-dione, 1-H) was developed [5–8]. Tryptanthrin is a tetracyclic moiety with colossal organic properties like anticancer, antibacterial, antifungal, antitumor antimalarial, antiparasitic. Due to not insignificant rundown of bio-properties related to this tetracyclic moiety has endorsed the investigation of large numbers of its structural isomer. Here, we have synthesized tryptanthrin by condensation of isatoic anhydride with isatin in the presence of triethylamine using toluene as a solvent [9]. This method was chosen due to readily available starting materials for the synthesis of tryptanthrin for environmental implications and operational simplicity.

Schiff bases are organic molecules with biologically active azomethine groups and were explored by many researchers[10–12]. The Schiff base's metal complexes have better biological activity than the organic molecule. Platinum(II) complexes, which are pre-owned as anticancer drugs, including cisplatin, oxaliplatin, nedaplatin carboplatin, and iproplatin, have a certain limitation comes after experience of

their incorporation in the human body [13–15]. The mechanism of action of the platinum-based anticancer agent has a role of N, N-donor ligand that makes the strong coordinate bond with Pt(II) ion and two labile coordinating chloride ion, the good leaving properties of which permit positively charged platinum(II) ion to interact with negatively charged DNA molecule base pair [16, 17]. With an interest in exploring the biological interactions of Pt(II) complexes, we have synthesized Pt(II) complexes with heterocyclic ligands tryptanthrin and performed many spectral, computational and biological studies.

Results And Discussion

Proton NMR and IR spectroscopy

Aromatic protons of the ligands (L^1-L^7) are observed in the range of 7.11 – 8.53 δ ppm shifted to 7.14 – 8.49 δ ppm as a counter effect of chelation in case of the complexes (I-VII). N-H proton of ligands is observed in the range of 13.34-13.50 δ ppm, which are shifted to 13.41-13.45 δ ppm in platinum(II) complexes. Shifting of signal in case of metal complexes is observed due to coordination of metal ion with the ligand [18].

IR frequency of platinum(II) complexes (I-VII) is slightly switched higher than respective ligands (L^1-L^7). In all synthesized compounds, frequency of $\nu(C=C)_{aromatic}$ is observed at 1478-1494 cm^{-1} and 1608-1621 cm^{-1}, respectively. The signal at 1607-1617 cm^{-1} and 1665-1687 cm^{-1} frequency of tryptathrin in ligand and complexes (I-VII) are due to $\nu(C=O)_{stretching}$. Ligands (L^1-L^7) and Pt(II) complexes (I-VII) show a frequency of $\nu(C=N)_{ar.\ stretching}$ at around 1611-1618 cm^{-1} and 1488-1596 cm^{-1}, respectively. (All NMR, mass spectrum, and IR spectrum shown in electronic supplementary material no.1)

Electronic spectra, magnetic behaviour and conductance measurement

To confirm the geometry of synthesized Pt(II) complexes. Three bands in 257-268 nm, 367-391 nm, and 316-332 nm appear in the electronic spectra of platinum complexes due to MLCT transition, d-d transition, and charge transfer transition, respectively. The calculated effective magnetic moment value for the platinum(II) complexes is zero BM, which confirms the square planar geometry for platinum(II) complexes with dsp^2 hybridization and the diamagnetic nature of complexes. Furthermore, the value of the molar conductance of the complexes is 14.57 - 22.61 Ω^{-1} cm^2 mol^{-1}, which confirms the non-ionic nature of the complex.

DFT study

HOMO-LUMO energy gap

The HOMO-LUMO energy gap is a key factor in studying various physical properties of metal complexes, one of which is a prediction of biological activity. The molecule's stability depends on the HOMO-LUMO energy gap, and the reactivity is inversely proportional to that. A molecule with little orbital energy gap is usually more active [19]. The energy gap of the tryptathrin based Pt(II) complexes are in the 2.358 to

2.587 eV. From Table.1, we can see that complexes III should have a higher bioactivity than the other complexes because it has a lower energy gap, which is also confirmed by the cytotoxicity on the MG -63 cell line and BSLB. From Fig. 1, we can conclude that the central Pt atom is covered by HOMO electron cloud with the chloride group, whereas the ligand's moiety is covered by LUMO electron cloud so LMCT occurs in the excitation of the complex. (The optimized bond length and bond angles, Mulliken charges, optimized electronic structure, HOMO-LUMO electron cloud image of all complexes are shown in electronic supplementary material no. 2)

Table 1. HOMO-LUMO energy of the Pt(II) complexes

Complex	HOMO Energy		LUMO Energy		E_{LUMO}-E_{HOMO}
	Hartree	eV	Hartree	eV	eV
I	-0.233	-6.333	-0.138	-3.752	2.582
II	-0.237	-6.454	-0.143	-3.902	2.552
III	-0.237	-6.436	-0.143	-3.886	2.551
IV	-0.231	-6.277	-0.144	-3.919	2.358
V	-0.237	-6.460	-0.143	-3.895	2.564
VI	-0.237	-6.440	-0.142	-3.874	2.566
VII	-0.231	-6.290	-0.136	-3.703	2.587

Mulliken population analysis

Mulliken population analysis (MPA) represents the atomic charge of the complexes. The highest negative and positive charges are shown in Table 2.

Table 2. Mulliken charge of the Pt(II) complexes(I-VII)					
I	N35(-0.385605)	N31(-0.32645)	O33(-0.227794)	N34(-0.214402)	Cl42(-0.139772)
	Pt41(0.160492)	C12(0.173697)	C13(0.203068)	C3(0.240562)	C20(0.330273)
II	N34(-0.385468)	N30(-0.328101)	O32(-0.226546)	N33(-0.213821)	Cl41(-0.138676)
	Pt40(0.159813)	C12(0.174329)	C13(0.203251)	C3(0.23941)	C20(0.338865)
III	N34(-0.385447)	N30(-0.328459)	C23(-0.232961)	O32(-0.226622)	N33(-0.213867)
	Pt40(0.161018)	C12(0.174195)	C13(0.203215)	C3(0.239596)	C20(0.337036)
IV	N34(-0.385655)	N30(-0.326256)	C24(-0.234064)	O32(-0.22827)	N33(-0.214539)
	C12(0.173044)	C13(0.203018)	C3(0.240837)	C20(0.319922)	C23(0.430243)
V	N34(-0.38724)	N30(-0.324674)	O32(-0.227386)	N33(-0.211453)	Cl41(-0.135748)
	Pt40(0.163877)	C11(0.177322)	C12(0.203001)	C3(0.239296)	C19(0.33071)
VI	N34(-0.38663)	N30(-0.324618)	C5(-0.262323)	O32(-0.227439)	N33(-0.212027)
	Pt40(0.162483)	C11(0.176268)	C12(0.203043)	C3(0.240107)	C19(0.330764)
VII	N34(-0.386652)	N30(-0.327184)	O32(-0.229133)	N33(-0.211414)	C4(-0.176048)
	C11(0.172914)	C12(0.201888)	C3(0.240081)	C19(0.331244)	C5(0.389664)

Here we can identify plausible biomolecular interaction utilizing the molecular electrostatic potential (ESP) cloud picture over the structure, which is produced using the Mulliken charges of the atom. Image generated from the docking output file shows that the molecule's interaction with the DNA is done mainly via atoms that possess the most elevated electropositive and electronegative charge. The optimized structure of the Pt(II) metal complex and the image of the electrostatic potential present in complex-I is shown in Fig. 2.

Molecular docking study

Theoretically, we can predict the interaction of synthesized compounds with macromolecules using the computational method. A molecular docking study provides a good platform for finding binding energy of synthesized molecules with the macromolecule[20]. The negative value of docking energy, indicates more binding affinity of synthesized molecules with DNA macromolecule. In case of HEX software, the binding energy of ligands is varies from -274.52 to -258.26 kJ/mol and Pt(II) complexes is in the range of -290.02 to -278.2, kJ/mol, while in case of the auto dock vina, binding energy of ligands varies from 7.9 to 8.2 and Pt(II) complexes is in the range of 8.1 to 8.4 kCal/mol. From the output of docking software, it can be conclude that metal complexes have a more affinity to bind with DNA molecule than ligands [21]. Which is also supported by our prediction that chelation of the organic ligand with metal ions increases the bio-property of the complexes.

Visualization of docking with the discovery studio says that the ligand molecule interacts with the DNA guanine residue. Two hydrogen bonds are formed between the compound and DNA molecule; pi donor H-bond interaction is shown between the aromatic ring of the tryptathrin and DNA residue. 3D (A-C) and 2D (B) visualization of the docking is demonstrated in Fig. 3.

The molecular docking study with the topoisomerase II is used to predict the interaction of the synthesized molecule as the cancer inhibitor. Docking with topo II is performed using autodock vina and the results reveals that the Pt(II) complexes have more affinity to bind with inhibitor and it shown by the ligplot as the output visualization of the docking study. In case of the complex I main interaction is occurring through the LEU66, ALA399, GLN387, SER65, HIS393, ASP397, ASP61, LYS64, LYS38, SER 62, SER400, TRY403 residue (Fig.4 B). In case of complexes, the number interaction is fourteen and the type of interaction with residue is six, while in case of corresponding ligands the number interaction is reduce to twelve and the type of interaction with residue is reduce to three only.

Biological study of synthesized compounds

Bacteriostatic activity

When the free organic moiety makes a coordination compound with the metal, its lipophilicity increases by the polarizability of metal ion, which reduces by the L→M donation. It also provides delocalization for electrons according to Tweedy's chelation principle. Lipophilicity plays a vital role in membrane permeation microorganisms. With an increase in lipophilicity, penetration of drug molecules will become accessible in the cell through the cell membrane. So, the nature of the ligands and chelate effects have a key role in the bacteriostatic activity of the metal complexes. In synthesized ligands, L^2, $L^{3,}$ and L^5 show better antibacterial activity than ligands L^1, L^4, L^6, and L^7. Complexes I, III, and V show less MIC value than II, IV, and VI. The bacteriostatic activity was performed using the broth dilution method reported in the literature [22]. Here Ciprofloxacin drug is used as a standard antibiotic for antibacterial study.

Anticancer activity against MG-63 cell line

Anticancer activity was performed to measure the extent of potency for the compound on human bone cancer cell lines (MG-63). To quantify the cytotoxicity of the synthesized compound, MTT assay colourimetric method was used [23]. All the synthesized compounds show some percentage viability on the cancer cell line. Like dose-dependent manner, all the compounds show somewhat cytotoxicity on the cancer cell line. IC_{50} values of ligands are higher than the respective complex means metal complexes are more potent than ligands against the cancer cell line (MG-63). The potency of the ligands is increased on complexation. IC_{50} value of the platinum(II) complexes and ligands is observed in the range of 10.9 µg/mL to 18.2 µg/mL and 19.5 µg/mL to 28.7 µg/mL, respectively. IC_{50} value of the complex III (10.9 µg/mL is comparable to cisplatin (10 µg/mL) [24]. In case of the complex III, there is a bromine atom present at the *p*-position of the phenyl ring, and due to its electron-withdrawing nature, it shows more potency against the cancer cell line (MG-63).

In vivo brine shrimp lethality bioassay (BSLB)

In the process of step-by-step drug development, pharmacological exercise is a very crucial step. Brine shrimp are easily available, cheap, and easy to handle organisms. So, in drug development, it is used as a model for cytotoxic study. The value of the 50 % mortality is defined as LC_{50} of the compound. The order of the LC_{50} value for the synthesized ligands and metal complexes are: Cis-Platin < III< V <II < VI < VII < I < IV < L^5 < L^2 < L^6 < L^6 < L^1 < L^3 < L^7 < L^4, Complexes I and V show potent cytotoxicity activity than complexes II, III, IV, and VI. In the case of ligands, L^1 and L^3 exhibit more potent cytotoxicity activity than L^2, L^4, L^5, and L^6. LC_{50} values of heterocyclic agents and Pt(II) complexes are observed in the range of 9.24-11.18 µg/mL and 5.9-7.94, respectively, which is comparable to reported metal complexes[25]. In the case of cisplatin, the LC_{50} value is 3.15 µg/mL [26]. In the case of the synthesized compound, the LC_{50} value is in the range of 5.9-7.94 µg/mL, so it is less toxic than cisplatin [34]. Still, the anticancer activity of the synthesized compound is comparable to antineoplastic agent cisplatin.

DNA binding studies

Electronic absorption titration study

CT-DNA (Calf Thymus DNA) was used to study the binding interaction with synthesized molecules using the reported method in the literature. Tryptanthrin based ligands (L^1-L^7), and platinum(II) complexes (I-VII) exhibit hypochromism shift and bathochromic shift, which shows non-covalent interaction (i.e. intercalation) types of binding with K_b value in a range of $0.22 \times 10^5 – 2.90 \times 10^5$ M^{-1}. Binding affinity order of ligands (L^1-L^7), and platinum complexes (I-VII) are: IV> I > II > III > V > VI > L^4 > L^1 > L^5 > L^3 > L^2 > L^6. Binding constant values of the Pt(II) complexes are higher than respective ligands, which shows that the Pt(II) complexes bind more strongly with the CT-DNA than the respective ligands. Also, The K_b values of complexes (I-VII) are comparable with reported complexes[27]. The K_b value graph of ligand (L^1), shown in Fig. 6, and K_b value of all compounds are shown in Table 3.

Fluorescence quenching studies with DNA

Mode of DNA binding can be studied using DNA binding dye as several dyes have been well studied, and their binding modes are well established. Assuming that any molecule replaces a DNA-bound dye will probably bind with the DNA at that specific target. The intensity of the fluorescence from DNA- ethidium bromide complex dwindles as the added molecule replaces it. In the case of the ligands and complexes, more quenching of the intensity of the fluorescence is observed in the metal complexes, hence more substitution places in case of the metal complexes. The value of K_{sv} is shown in Table 3, which is in the range of $0.74– 1.94 \times 10^3$ M^{-1}.

Table 3. Biological activity data of ligands(L^1-L^7) and complexes(I-VII)

	DNA binding (K_b) × 10^5 M^{-1}	K_{sv} × 10^3 M^{-1}	BSA binding (K_b) × 10^4 M^{-1}	K_{sv} ×10^3 M^{-1}
L^1	0.65	0.76	0.63	0.42
L^2	0.8	0.93	0.73	0.56
L^3	0.71	0.84	0.64	0.49
L^4	0.57	0.74	0.52	0.37
L^5	0.95	1.03	0.85	0.69
L^6	0.84	0.97	0.75	0.6
L^7	0.68	0.81	0.61	0.62
I	1.14	1.23	1.02	0.63
II	1.51	1.61	1.37	0.8
III	1.39	1.52	1.26	0.71
IV	1.07	1.24	0.97	0.57
V	1.81	1.94	1.62	0.95
VI	1.65	1.77	1.48	0.84
VII	1.27	1.42	1.14	0.68

Viscosity measurements

Viscosity measurement is a sensitive technique to find the interaction of the compound with DNA So, viscosity measurement was performed to confirm the binding mode of the synthesized compound with the DNA molecule. The molecule can alter the viscosity of DNA solution through interaction with the DNA base pair. When any molecule intercalates between two base pairs, it will increase the viscosity of the DNA solution [28]. The result of the viscosity measurement is concluded in a coaxial graph of the relative viscosity i.e.$(\eta/\eta^0)^{1/3}$ vs. [complex]/[DNA]. Order of viscosity for compounds is VI > II > V > VII > IV> III > I > L^3 > L^1 > L^4 > L^2 > L^5 > L^7 > L^6. An increase in viscosity CT-DNA with a higher concentration of compounds indicates intercalation binding.

BSA binding studies

Absorption titration study

BSA (Bovine Serum Albumin) is a useful macromolecule in the drug development study due to its structural homology with HSA (Human Serum Albumin). UV-Visible absorption titration of BSA was

performed by increasing the amount of the ligands (L^1 – L^7), and Pt(II) complexes (I-VII) at 250-550 nm wavelength range [29]. An increase in the band's intensity without any change of position was observed. The K_b values of ligands (L^1 – L^7), and Pt(II) complexes (I-VII) are observed in the range of 0.41 – 1.18 × 10^4 and 0.99 – 1.63 × 10^4, respectively. The K_b value of the ligands and Pt(II) complexes demonstrate their moderate activity.

So, we can say that they can carry the molecule in the body of the leaving organism in the case of a drug delivery study. All K_b value is shown in Table 3, and a representative graph of the ligand1(L^1) is shown in Fig. 7

Fluorescence quenching study with BSA

In the field of drug discovery, we can say that the interaction of the synthesized compounds with biomolecules is more important. Bovine serum albumin is a model for drug discovery as it has structural similarities with human serum albumin. The fluorescence spectra of the BSA give 280 nm as an exciting wavelength in a spectrofluorometer. By the successive addition of the metal complexes solution, the emission intensity of the BSA is quenched, mainly from the three intrinsic components, tyrosine, tryptophan, and phenylalanine residue. Stern–Volmer plot drawn from the data gives liner relationship representing excellent affinity of all synthesized complexes to bind with BSA Stern Volmer constant K_{sv}, binding constant (K_a), and binding sites(n) are in the range of 1.07 – 2.80×10^3 M^{-1}, 0.10 – 0.58 × 10^5 M^{-1}, and 0.92 – 1.12, respectively. The binding constant K_a of platinum(II) complexes order : I < VII < II < V < VI< IV < III.

Conclusions

Tryptathrin alkaloid-based N, N-donor ligands and its Pt(II) complexes were synthesized and characterized by various techniques (^{1}H NMR, Mass, IR, Elemental analysis, UV-vis.). The shifting of signals in the ^{1}H NMR spectra and IR frequencies support the formation of Pt(II) complexes. Optimized structures from DFT suggest square planar geometry. Complex IV has the highest HOMO-LUMO gap – 2.6299 eV. Pt(II) complex III possesses a Lower HOMO-LUMO gap(2.551 eV), showing anticancer activity comparable to standard drug *cis*-platin. From the UV-visible absorption titration, it can be concluded that the synthesized molecule interacts with the CT-DNA with non-covalent binding, particularly through the intercalation mode of binding, which is supported by viscosity measurement and docking study of the Pt(II) complexes. Therefore, Complex-DNA binding energy and binding efficacy are higher than the corresponding ligand. Platinum(II) complexes show a lower MIC value than the corresponding ligand against the bacterial species, which indicates complexes exhibit higher potency in bacteriostatic activity. In the case of the anticancer activity against cancer cell line (MG-63), platinum(II) complexes have lower IC_{50} values. Complex III has a comparable IC_{50} value(10.91 µg/mL) with standard drug cisplatin (10 µg/mL). Complex III also has lower cytotoxicity against brine shrimp, overcoming the limitation of higher toxicity of cisplatin as a standard drug.

Experimental Portion

Preparation of tryptanthrin Schiff base based N, N- donor ligands (L^1-L^7) and Pt(II)metal complexes

- Synthesis of the tryptanthrin (indolo[2,1-b]quinazoline-6,12-dione, 1-H) was done by adding solution of the isatoic anhydride to the boil solution of the toluene followed by refluxing the reaction mixture for 60–70 min [9]. The precipitated product was washed with methanol and used for further reaction. Schiff base of the tryptanthrin was obtained through stirring the equimolar amount of the tryptanthrin and substituted phenylhydrazine hydrochloride in methanol at room temperature for 4–6 hours. The crude was filtered, washed with methanol, and recrystallized from a mixture of methanol and chloroform. Metal complexes of the tryptathrin based ligand were prepared by adding methanolic solution of ligand into K_2PtCl_4 solution in methanol and reflux for 2–3 h and then stirred at RT for 20 h.[30]

Characterization Data

(E)-6-(2-Phenylhydrazineylidene)indolo[2,1-b]quinazolin-12(6H)-one (L^1)

- Empirical formula: $C_{21}H_{14}N_4O$; % Yield:79.82; Color: Orange fluffy solid; M.P.: >300°C; M.W.:338.37 gm/mol; calc.(%): C, 74.54; H, 4.17; N, 16.56; Found. (%): C, 74.43; H, 4.28; N, 16.62; m/z(%):338 (100) $[M]^+$, 339 [M + 1]; ^{1}H NMR (400 MHz, $CDCl_3$) δ/ppm: 13.37 (1H, s, $H_{2'}$), 8.52 (1H, d, J = 8Hz, H_2), 8.40 (1H, d, J = 7.6Hz, H_5), 7.71–7.81 (3H, m $H_{5',6',7'}$), 7.51 (1H, t, J = 7.6Hz H_3), 7.28–7.44 (6H, m, $H_{7, 8, 9, 10, 4', 8'}$), 7.11(1H, t, J = 8Hz, H_4); IR(4000–450 cm^{-1}): 3051 ν(= C-H) $_{Stretchig}$ 1580 $\nu(C = N)_{Stretching}$, 1609 $\nu(C = O)_{Stretching}$, 1478 $\nu(C = C)_{ar.\ Stretching}$, 1171 $\nu(C\text{-}N)_{Stretching}$.

(E)-6-(2-(4-Chlorophenyl)hydrazineylidene)indolo[2,1-b]quinazolin-12(6H)-one (L^2)

Empirical formula: $C_{21}H_{13}ClN_4O$; % Yield: 76.32; Color: yellowish fluffy solid; M.P.: >300°C; M.W.: 372.82 gm/mol.; calc.(%): C, 67.66; H, 3.51; N, 15.03; Found. (%):C, 67.78; H, 3.60; N, 14.94; m/z(%):372 (100) [M]+, 374 [M + 2]; ^{1}H NMR (400 MHz, $CDCl_3$) δ/ppm: 13.50 (1H, s, $H_{2'}$), 8.53 (1H, d, J = 8Hz, H_2), 8.47 (1H, d, J = 7.6Hz, H_5), 7.81–7.86 (3H, m $H_{5',7',8}$), 7.59 (1H, t, J = 7.0Hz H_3), 7.40–7.52 (5H, m, $H_{7, 9, 10, 4', 8'}$), 7.16(1H, t, J = 8Hz, H_4); IR Spectra (KBr, 4000–450 cm^{-1}) 3050 $\nu(= C\text{-}H)_{ar.\ Stretching}$, 1605 $\nu(C = O)_{Stretching}$, 1586 $\nu(C = N)_{ar.\ Stretching}$, 1483 $\nu(C = C)_{ar.\ Stretching}$, 1396 $\nu(C\text{-}N)_{ar.\ Stretching}$, 748 $\nu(= C\text{-}H)_{bending,}$ 663 $\nu(C\text{-}H)_{bending}$ 556 ν(C-Cl).

(E)-6-(2-(4-Bromophenyl)hydrazineylidene)indolo[2,1-b]quinazolin-12(6H)-one (L^3)

Empirical formula: $C_{21}H_{13}BrN_4O$; %Yield:79.15, Color: Dark yellowish fluffy solid; M.P.: >300°C; M.W.: 417.27; gm/mol calc. (%):C, 60.45; H, 3.14; N, 13.43; Found. (%):C, 60.57; H, 3.26; N, 13.54; m/z(%):417 (100) [M]+, 419 [M + 2] (95); ^{1}H NMR (400 MHz, $CDCl_3$) δ/ppm: 13.49 (1H, s, $H_{2'}$), 8.53 (1H, d, J = 8Hz, H_2), 8.47 (1H, d, J = 7.6Hz, H_5), 7.60–7.85 (3H, m $H_{5',7',8}$), 7.59 (1H, t, J = 7.0Hz H_3), 7.40–7.58 (5H, m, $H_{7,9,10,4',8'}$), 7.16(1H, t, J = 8Hz, H_4); IR Spectra (KBr, 4000–450 cm^{-1}) 3048 v(= C-H)$_{ar.\ Stretching}$, 1605 v(C = O)$_{Stretching}$, 1585 v(C = N)$_{ar.\ Stretching}$, 1480 v(C = C)$_{ar.\ Stretching}$, 1395 v(C-N)$_{ar.\ Stretching}$, 818 v(C-Br)$_{stretching}$, 754 v(= C-H)$_{bending,}$ 663 v(C-H)bending

(E)-6-(2-(p-Tolyl)hydrazineylidene)indolo[2,1-b]quinazolin-12(6H)-one (L^4)

Empirical formula: $C_{22}H_{16}N_4O$; %Yield: 89.11; Color: yellowish fluffy solid;M.P.: >300°C; M.W.: 352.4 gm/mol; calc. (%):C, 74.98; H, 4.58; N, 15.90; Found. (%):C, 74.89; H, 4.65; N, 15.84; m/z(%):352 (100) $[M]^+$, ^{1}H NMR (400 MHz, $CDCl_3$) δ/ppm: 13.34 (1H, s, $H_{2'}$), 8.35 (2H, m, $H_{2,5}$), 7.79–7.55 (3H, m, $H_{3,4,8}$), 7.51(1H, t, J = 6.4Hz H_9) 7.32-7. 46 (4H, m, $H_{4',5',7',8'}$),7.00-7.24 (2H, m, $H_{7,10}$), 2.44(3H, s, -CH_3); IR Spectra (KBr, 4000–400 cm^{-1}): IR Spectra (KBr, 4000–450 cm^{-1}) 3042 v(= C-H)$_{ar.\ Stretching}$, 1607 v(C = O)$_{Stretching}$, 1588 v(C = N)$_{ar.\ Stretching}$, 1481 v(C = C)$_{ar.\ Stretching}$, 1389 v(C-N)$_{ar.\ Stretching}$, 755 v(= C-H)$_{bending,}$ 661 v(C-H)$_{bending}$.

(E)-8-Chloro-6-(2-phenylhydrazineylidene)indolo[2,1-b]quinazolin-12(6H)-one (L^5)

Empirical formula: $C_{21}H_{13}ClN_4O$; %Yield: 89.11; Color: yellowish fluffy solid; M.P.: >300°C; M.W.: 372.82gm/mol; calc. (%):C, 67.66; H, 3.51; N, 15.03; Found. (%):C, 67.73; H, 3.59; N, 15.11; m/z(%):372 (100) $[M]^+$, 374 [M + 2] ; ^{1}H NMR (400 MHz, $CDCl_3$) δ/ppm: 13.50 (1H, s, $H_{2'}$), 8.53 (1H, d, J = 8Hz, H_2), 8.47 (1H, d, J = 7.6Hz, H_5), 7.81–7.86 (3H, m $H_{5',7',8}$), 7.59 (1H, t, J = 7.0Hz H_3), 7.40–7.52 (5H, m, $H_{7,9,10,4',8'}$), 7.16(1H, t, J = 8Hz, H_4); IR Spectra (KBr, 4000–400 cm^{-1}): IR Spectra (KBr, 4000–450 cm^{-1}) 3053 v(= C-H)$_{ar.\ Stretching}$, 1615 v(C = O)$_{Stretching}$, 1489 v(C = C)$_{ar.\ Stretching}$, 1578 v(C = N)$_{ar.\ Stretching}$, 1396 v(C-N)$_{ar.\ Stretching}$, 753 v(= C-H)$_{bending,}$ 656 v(C-H)$_{bending}$.

- **(E)-8-Bromo-6-(2-phenylhydrazineylidene)indolo[2,1-b]quinazolin-12(6H)-one (L^6)** Empirical formula: $C_{21}H_{13}BrN_4O$ %Yield: 89.11; Color: yellowish fluffy solid; M.P.: >300°C; M.W.: 417.27gm/mol; calc. (%):C, 60.45; H, 3.14; N, 13.43; Found. (%):C, 60.53; H, 3.23; N, 13.51; m/z(%):417 (100) $[M]^+$, 419 [M + 2] ; ^{1}H NMR (400 MHz, $CDCl_3$) δ/ppm: 13.48 (1H, s, $H_{2'}$), 8.40–8.50 (2H, m, $H_{8,7}$), 8.01 (1H, s, H_{10}), 7.81–7.87 (2H, m $H_{2,3}$), 7.52–7.59 (2H, m, $H_{4,5}$), 7.43–7.58 (4H, m, $H_{4',5',7',8'}$), 7.16(1H, t, J = 7.6Hz, $H_{6'}$); IR Spectra (KBr, 4000–450 cm^{-1}) 3048 v(= C-H)$_{ar.\ Stretching}$, 1612 v(C = O)$_{Stretching}$, 1492 v(C =

C)$_{ar.\ Stretching}$, 1586 v(C = N)$_{ar.\ Stretching}$,1395 v(C-N)$_{ar.\ Stretching}$, 753 v(= C-H)$_{bending,}$ 817 v(C-Br)$_{stretching}$, 663 v(C-H)$_{bending}$

(E)-8-Methyl-6-(2-phenylhydrazineylidene)indolo[2,1-b]quinazolin-12(6H)-one (L^7)

Empirical formula: $C_{22}H_{16}N_4O$ %Yield: 89.11; Color: yellowish fluffy solid; M.P.: >300°C; M.W.: 352.4 gm/mol; calc. (%):C, 74.98; H, 4.58; N, 15.90; Found. (%):C, 74.87; H, 4.64; N, 15.82; m/z(%):352 (100) $[M]^+$; ^{1}H NMR (400 MHz, $CDCl_3$) δ/ppm: 13.46 (1H, s, $H_{2'}$), 8.38–8.53 (2H, m, $H_{8,7}$), 7.7 (1H, s, H_{10}), 7.75–7.86 (2H, m $H_{2,3}$), 7.31–7.60 (4H, m, $H_{4', 5', 7', 8'}$), 7.23–7.29 (2H, m, $H_{4,5}$), 7.16(1H, t, J = 7.2Hz, $H_{6'}$) 2.49 (3H, s, -CH_3); IR Spectra (KBr, 4000–400 cm^{-1}):) 3046 v(= C-H)$_{ar.\ Stretching}$, 1613 v(C = O)$_{Stretching}$, 1496 v(C = C)$_{ar.\ Stretching}$, 1582 v(C = N)$_{ar.\ Stretching}$, 1393 v(C-N)$_{ar.\ Stretching}$, 754 v(= C-H)$_{bending}$, 663 v(C-H)$_{bending}$.

$[Pt(L^1)Cl_2]$ (I)

Empirical formula: $C_{21}H_{14}Cl_2N_4OPt$ %Yield: 59.78; Color: black solid; M.P.: > 300°C; M.W.: 604.35 gm/mol; Conductance: 18.72 $ohm^{-1}cm^2mol^{-1}$; ^{1}H NMR (400 MHz, DMSO-d_6) δ/ppm: 13.44 (1H, s, $H_{2'}$), 8.49 (1H, d, J = 6.4Hz, H_2), 8.36 (1H, d, J = 7.2Hz, H_7), 8.14 (1H, d, J = 6.8Hz, H_5), 7.86–8.01 (2H, m $H_{10,3}$), 7.25–7.77 (7H, m, $H_{8, 9, 4', 5',6', 7', 8'}$), 7.14(1H, t, J = 6.4Hz, H_4); IR Spectra (KBr, 4000–450 cm^{-1}) 3087 v(= C-H)$_{ar.\ Stretching}$, 1673 v(C = O)$_{Stretching}$,1611 v(C = N)$_{ar.\ Stretching}$,1608 v(C = C)$_{ar.\ Stretching}$, 1392 v(C-N)$_{ar.\ Stretching}$, 753 v(= C-H)$_{bending,}$ 663 v(C-H)$_{bending,}$555 v(Pt-N).

$[Pt(L^2)Cl_2]$ (II)

Empirical formula: $C_{21}H_{13}Cl_3N_4OPt$; %Yield: 57.43 Color: black solid; M.P.: > 300°C M.W.: 638.80 gm/mol; Conductance: 14.57 $ohm^{-1}cm^2mol^{-1}$; ^{1}H NMR (400 MHz, DMSO-d_6) δ/ppm: 13.43 (1H, s, $H_{2'}$), 8.48 (1H, d, J = 6.4Hz, H_2), 8.35 (1H, d, J = 7.2Hz, H_7), 8.16 (1H, d, J = 6.8Hz, H_5), 7.91–8.04 (2H, m $H_{10,3}$), 6.44–7.78 (7H, m, $H_{4, 8, 9, 4', 5', 7', 8'}$); IR Spectra (KBr, 4000–450 cm^{-1}): 3092 v(= C-H)$_{ar.\ Stretching}$, 1665 v(C = O)$_{Stretching}$, 1619 v(C = C)$_{ar.\ Stretching}$, 1613 v(C = N)$_{ar.\ Stretching}$, 1392 v(C-N)$_{ar.\ Stretching}$, 817 v(C-Br)$_{stretching}$, 753 v(= C-H)$_{bending,}$ 663 v(C-H)$_{bending,}$ 524 v(Pt-N) .

$[Pt(L^3)Cl_2]$ (III)

Empirical formula: $C_{21}H_{13}BrCl_2N_4OPt$ %Yield: 56.86, Color: dark brown crystalline solid; M.P.: > 300°C M.W.: 683.25 gm/mol; Conductance: 18.35 $ohm^{-1}cm^2mol^{-1}$; ^{1}H NMR (400 MHz, DMSO-d_6) δ/ppm13.41 (1H, s, $H_{2'}$), 8.49 (1H, d, J = 6.4Hz, H_2), 8.36 (1H, d, J = 7.6Hz, H_7), 8.17 (1H, d, J = 7.8Hz, H_5), 7.82–8.01 (3H, m $H_{3, 4, 8}$), 7.52–7.72 (5H, m, $H_{10, 4', 5', 7', 8'}$), 7.47(1H, t, J = 6.4Hz, H_9); IR Spectra (KBr, 4000–450 cm^{-1}): 3082 v(= C-H)$_{ar.\ Stretching}$, 1621 v(C = C)$_{ar.\ Stretching}$, 1668 v(C = O)$_{Stretching}$,1618 v(C = N)$_{ar.\ Stretching}$, 1392 v(C-N)$_{ar.\ Stretching}$, 817 v(C-Br)$_{stretching}$, 753 v(= C-H)$_{bending,}$ 663 v(C-H)$_{bending,}$ 570 v(Pt-N).

$[Pt(L^4)Cl_2]$ (IV)

Empirical formula: $C_{22}H_{16}Cl_2N_4OPt$ %Yield: 58.48, Color: black crystalline solid; M.P.: > 300°C M.W.: 618.38 gm/mol; Conductance: 22.61 $ohm^{-1}cm^2mol^{-1}$; ^1H NMR (400 MHz, DMSO-d_6) δ/ppm: 13.41 (1H, s, $H_{2'}$), 7.23–8.55 (12H, m, $H_{2,3,4,5,7,8,9,10,4',5',7',8'}$), 2.48 (3H, s,-$CH_3$); IR Spectra (KBr, 4000–450 cm^{-1}): 3085 $\nu(=C\text{-}H)_{ar.\ Stretching}$, 1671 $\nu(C=O)_{Stretching}$, 1613 $\nu(C=C)_{ar.\ Stretching}$, 1615 $\nu(C=N)_{ar.\ Stretching}$, 1392 $\nu(C\text{-}N)_{ar.\ Stretching}$, 753 $\nu(=C\text{-}H)_{bending,}$ 663 $\nu(C\text{-}H)_{bending,}$547 ν(Pt-N).

$[Pt(L^5)Cl_2]$ (V)

Empirical formula: $C_{21}H_{13}Cl_3N_4OPt$ %Yield: 59.78, Color: brown crystalline solid; M.P.: > 300°C M.W.: 638.80 gm/mol ; Conductance: 16.62 $ohm^{-1}cm^2mol^{-1}$; ^1H NMR (400 MHz, DMSO-d_6) δ/ppm: 13.41 (1H, s, $H_{2'}$), 8.49 (1H, d, J = 7.6Hz, H_2), 8.35 (1H, d, J = 6.4Hz, H_7), 8.16 (1H, d, J = 5.6Hz, H_5), 7.82–8.01 (3H, m $H_{4',6',8'}$), 7.40–7.78 (6H, m, $H_{5',7',3,4,8,10}$); IR Spectra (KBr, 4000–450 cm^{-1}): 3087 $\nu(=C\text{-}H)_{ar.\ Stretching}$, 1678 $\nu(C=O)_{Stretching}$,1617ν(C = C)$_{ar.\ Stretching}$, 1614ν(C = N)$_{ar.\ Stretching}$, 1392 $\nu(C\text{-}N)_{ar.\ Stretching}$, 753 $\nu(=C\text{-}H)_{bending,}$ 663 $\nu(C\text{-}H)_{bending,}$ 565 ν(Pt-N).

$[Pt(L^6)Cl_2]$ (VI)

Empirical formula: $C_{21}H_{13}BrCl_2N_4OPt$ %Yield: 57.24; Color: brown solid; M.P.: > 300°C M.W.: 683.25 gm/mol; Conductance: 15.62 $ohm^{-1}cm^2mol^{-1}$; ^1H NMR (400 MHz, DMSO-d_6) δ/ppm: 13.44 (1H, s, $H_{2'}$), 8.35–8.48 (2H, m, $H_{8,7}$), 8.56 (1H, s, H_{10}), 6.88–8.38 (9H, m $H_{2,3,4,5,4',5',6',7',8'}$); IR Spectra (KBr, 4000–450 cm^{-1}): 3084 $\nu(=C\text{-}H)_{ar.\ Stretching}$, 1687 $\nu(C=O)_{Stretching}$, 1620 $\nu(C=N)_{ar.\ Stretching}$, 1614 $\nu(C=C)_{ar.\ Stretching}$, 1392 $\nu(C\text{-}N)_{ar.\ Stretching}$, 817 $\nu(C\text{-}Br)_{stretching}$, 753 $\nu(=C\text{-}H)_{bending,}$ 663 $\nu(C\text{-}H)_{bending,}$ 573 ν(Pt-N).

$[Pt(L^7)Cl_2]$ (VII)

Empirical formula: $C_{22}H_{16}Cl_2N_4OPt$ %Yield: 54.61% Color: brown crystalline solid; M.P.: > 300°C M.W.: 618.38 gm/mol; Conductance: 19.56 $ohm^{-1}cm^2mol^{-1}$; ^1H NMR (400 MHz, DMSO-d_6) δ/ppm: 13.42 (1H, s, $H_{2'}$), 8.34–8.52 (2H, m, $H_{8,7}$), 7.32–7.83 (6H, m $H_{2,3,10,6'}$), 7.32–7.83 (4H, m, $H_{4,5,4',5',7',8'}$), 2.49 (3H, s, -CH_3); IR Spectra (KBr, 4000–450 cm^{-1}): 3079 $\nu(=C\text{-}H)_{ar.\ Stretching}$, 1683 $\nu(C=O)_{Stretching}$,1620 $\nu(C=C)_{ar.\ Stretching}$, 1612 $\nu(C=N)_{ar.\ Stretching}$, 1380 $\nu(C\text{-}N)_{ar.\ Stretching}$, 748 $\nu(=C\text{-}H)_{bending,}$ 667 $\nu(C\text{-}H)_{bending,}$ 570 ν(Pt-N).

Computational study

DFT

DFT study was performed on Gaussian 9 software package using B3LYP basis set as an L

nL2DZ function.

Docking

A molecular docking study was performed using HEX 8.0 program with windows 7 operating system. The optimized structure of the compounds from the DFT calculation was used as an input file in PDB format. For Autodock Vina PDBQT file was converted from the PDB file using MGL tools. A docking study was performed with grid dimension 98×58×56 Point (X×Y×Z).

Biological Study

Antibacterial and cytotoxicity study

Antibacterial study was performed using broth dilution method as reported in the literature[31]. Cytotoxicity study on the Artemia cyst is portrayed as the process reported by Meyer *et al.*,[32]

DNA binding study

According to previously published literature, all the binding studies, including DNA and BSA binding, using UV-visible and spectrofluorometer [27, 29]. DNA used for the binding study is CT-DNA and the concentration of the DNA used was 200μM which is calculated using the extinction coefficient(6600$M^{-1}cm^{-1}$) in Beer-Lambert Law.

Declarations

Acknowledgments

The authors are thankful to the Head, Department of Chemistry, Sardar Patel University, for providing necessary research facilities; DST-PURSE, Sardar Patel University, for LC-MS analysis; CAS-Phase-II and UGC-CPEPA program, Sardar Patel University for providing instrumental and chemicals facilities.

References

1. Abe T, Itoh T, Choshi T, Hibino S, Ishikura M (2014) One-pot synthesis of tryptanthrin by the Dakin oxidation of indole-3-carbaldehyde. Tetrahedron Lett 55(38):5268–5270. https://doi.org/10.1016/j.tetlet.2014.07.113
2. Kaur R, Manjal SK, Rawal RK, Kumar K (2017) Recent synthetic and medicinal perspectives of tryptanthrin. Bioorg Med Chem 25(17):4533–4552. https://doi.org/10.1016/j.bmc.2017.07.003
3. Schepetkin IA, Khlebnikov AI, Potapov AS, Kovrizhina AR, Matveevskaya VV, Belyanin ML et al (2019) Synthesis, biological evaluation, and molecular modeling of 11H-indeno[1,2-b]quinoxalin-11-one derivatives and tryptanthrin-6-oxime as c-Jun N-terminal kinase inhibitors [Internet]. Vol. 161, European Journal of Medicinal Chemistry.Elsevier Masson SAS;179–191p. https://doi.org/10.1016/j.ejmech.2018.10.023

4. Kamal A, Reddy BVS, Sridevi B, Ravikumar A, Venkateswarlu A, Sravanthi G et al (2015) Synthesis and biological evaluation of phaitanthrin congeners as anti-mycobacterial agents. Bioorg Med Chem Lett 25(18):3867–3872. https://doi.org/10.1016/j.bmcl.2015.07.057
5. Matveevskaya VV, Pavlov DI, Sukhikh TS, Gushchin AL, Ivanov AY, Tennikova TB et al (2020) Arene-Ruthenium(II) Complexes Containing 11 H-Indeno[1,2- b]quinoxalin-11-one Derivatives and Tryptanthrin-6-oxime: Synthesis, Characterization, Cytotoxicity, and Catalytic Transfer Hydrogenation of Aryl Ketones. ACS Omega 5(19):11167–11179. https://doi.org/10.1021/acsomega.0c01204
6. Tucker AM, Grundt P (2012) The chemistry of tryptanthrin and its derivatives. Arkivoc 2012(1):546–569. https://doi.org/10.3998/ark.5550190.0013.113
7. Onambele LA, Riepl H, Fischer R, Pradel G, Prokop A, Aminake MN (2015) Synthesis and evaluation of the antiplasmodial activity of tryptanthrin derivatives. Int J Parasitol Drugs Drug Resist 5(2):48–57. https://doi.org/10.1016/j.ijpddr.2015.03.002
8. Brandão P, Pinheiro D, Sérgio Seixas de Melo J, Pineiro M (2020) I2/NaH/DMF as oxidant trio for the synthesis of tryptanthrin from indigo or isatin. Dye Pigment 173 September 2019. https://doi.org/10.1016/j.dyepig.2019.107935
9. Amara R, Awad H, Chaker D, Bentabed-Ababsa G, Lassagne F, Erb W et al (2019) Conversion of Isatins to Tryptanthrins, Heterocycles Endowed with a Myriad of Bioactivities. Eur J Org Chem 2019(31–32):5302–5312. https://doi.org/10.1002/ejoc.201900352
10. Modi CK, Patel MN (2008) Synthetic, spectroscopic and thermal aspects of some heterochelates. J Therm Anal Calorim 94(1):247–255. https://doi.org/10.1007/s10973-007-8790-4
11. Patel NH, Parekh HM, Patel MN (2007) Synthesis, physicochemical characteristics, and biocidal activity of some transition metal mixed-ligand complexes with bidentate (NO and NN) Schiff bases. Pharm Chem J 41(2):78–81. https://doi.org/10.1007/s11094-007-0017-2
12. Abdel-Rahman LH, Abu-Dief AM, El-Khatib RM, Abdel-Fatah SM (2016) Some new nano-sized Fe(II), Cd(II) and Zn(II) Schiff base complexes as precursor for metal oxides: Sonochemical synthesis, characterization, DNA interaction, in vitro antimicrobial and anticancer activities. Bioorg Chem 69:140–152. https://doi.org/10.1016/j.bioorg.2016.10.009
13. Haribabu J, Tamizh MM, Balachandran C, Arun Y, Bhuvanesh NSP, Endo A et al (2018) Synthesis, structures and mechanistic pathways of anticancer activity of palladium(ii) complexes with indole-3-carbaldehyde thiosemicarbazones. New J Chem 42(13):10818–10832. https://doi.org/10.1039/c7nj03743k
14. Heidari L, Ghassemzadeh M, Fenske D, Fuhr O, Saeidifar M, Mohsenzadeh F (2020) Unprecedented palladium(ii) complex containing dipodal 1,3,4-thiadiazole derivatives: Synthesis, structure, and biological and thermal investigations. New J Chem 44(39):16769–16775. https://doi.org/10.1039/D0NJ02918A
15. Faghih Z, Neshat A, Wojtczak A, Faghih Z, Mohammadi Z, Varestan S (2018) Palladium (II) complexes based on Schiff base ligands derived from ortho-vanillin; synthesis, characterization and cytotoxic studies. Inorganica Chim Acta 471(Ii):404–412. https://doi.org/10.1016/j.ica.2017.11.025

16. Lazarević T, Rilak A, Bugarčić ŽD (2017) Platinum, palladium, gold and ruthenium complexes as anticancer agents: Current clinical uses, cytotoxicity studies and future perspectives. Eur J Med Chem 142:8–31. https://doi.org/10.1016/j.ejmech.2017.04.007
17. Kalaiarasi G, Aswini G, Rex Jeya Rajkumar S, Dharani S, Lynch VM, Prabhakaran R (2018) Synthesis, spectral, structural characterization and biological activity of new palladium(II) complexes containing 3-acetyl-8-methoxy-2H-chromen-2-one derived Schiff bases. Appl Organomet Chem 32(9). https://doi.org/10.1002/aoc.4466
18. Kim Y, Lee J, Son YH, Choi SU, Alam M, Park S (2020) Novel nickel(II), palladium(II), and platinum(II) complexes having a pyrrolyl-iminophosphine (PNN) pincer: Synthesis, crystal structures, and cytotoxic activity. J Inorg Biochem 205(January):111015. https://doi.org/10.1016/j.jinorgbio.2020.111015
19. Basava Punna Rao A, Gulati K, Joshi N, Deb DK, Rambabu D, Kaminsky W et al (2017) Synthesis and biological studies of ruthenium, rhodium and iridium metal complexes with pyrazole-based ligands displaying unpredicted bonding modes. Inorganica Chim Acta 462:223–235. https://doi.org/10.1016/j.ica.2017.03.037
20. Pandya SB, Socha BN, Chaudhary KP, Dubey RP, Chavda BR, Patel UH et al (2020) Combined experimental and computational studies on molecular structure of nickel complex of 4-amino-N-(1, 3-thiazol-2-yl) benzenesulfonamide with coordinated pyridine. Inorg Nano-Metal Chem 0(0):1–11. https://doi.org/10.1080/24701556.2020.1835965
21. Karami K, Alinaghi M, Amirghofran Z, Lipkowski J (2018) Synthesis and characterization of two new trans palladium (II) complexes containing benzylamine ligand: DNA/BSA interactions, molecular docking and in vitro cytotoxic activity. Inorganica Chim Acta 471(Ii):797–807. https://doi.org/10.1016/j.ica.2017.02.027
22. Patel MN, Patel CR, Joshi HN (2013) Synthesis, characterization and biological studies of mononuclear copper (II) complexes with cipro fl oxacin and N, O donor ligands. Inorg Chem Commun 27:51–55. https://doi.org/10.1016/j.inoche.2012.10.018
23. Yamali C, Gul HI, Ece A, Bua S, Angeli A, Sakagami H et al (2019) Synthesis, biological evaluation and in silico modelling studies of 1,3,5-trisubstituted pyrazoles carrying benzenesulfonamide as potential anticancer agents and selective cancer-associated hCA IX isoenzyme inhibitors. Bioorg Chem 92(August):103222. https://doi.org/10.1016/j.bioorg.2019.103222
24. Altaf M, Casagrande N, Mariotto E, Baig N, Kawde AN, Corona G et al (2019) Potent in vitro and in vivo anticancer activity of new bipyridine and bipyrimidine gold (III) dithiocarbamate derivatives. Cancers (Basel) 11(4):1–14. https://doi.org/10.3390/cancers11040474
25. Varma RR, Pandya JG, Sharma J, Pathak C, Patel MN (2020) DNA interaction, in vivo and in vitro cytotoxicity, reactive oxygen species, lipid peroxidation of –N, S donor Re(I) metal complexes. Mol Divers. https://doi.org/10.1007/s11030-020-10040-2. ;(I)
26. Patel NJ, Bhatt BS, Vekariya PA, Vaidya FU, Pathak C, Pandya J et al (2020) Synthesis, characterization, structural-activity relationship and biomolecular interaction studies of heteroleptic

Pd(II) complexes with acetyl pyridine scaffold. J Mol Struct 1221(Ii):128802. https://doi.org/10.1016/j.molstruc.2020.128802

27. Shanmugapriya A, Kalaiarasi G, Kalaivani P, Dallemer F, Prabhakaran R (2016) CT-DNA/BSA protein binding and antioxidant studies of new binuclear Pd(II) complexes and their structural characterisation. Inorganica Chim Acta 449:107–118. https://doi.org/10.1016/j.ica.2016.05.018
28. Sankarganesh M, Vijay Solomon R, Dhaveethu Raja J (2021) Platinum complex with pyrimidine- and morpholine-based ligand: synthesis, spectroscopic, DFT, TDDFT, catalytic reduction, in vitro anticancer, antioxidant, antimicrobial, DNA binding and molecular modeling studies. J Biomol Struct Dyn 39(3):1055–1067. https://doi.org/10.1080/07391102.2020.1727364
29. Franich AA, Živković MD, Milovanović J, Arsenijević D, Arsenijević A, Milovanović M et al (2020) In vitro cytotoxic activities, DNA- and BSA-binding studies of dinuclear palladium(II) complexes with different pyridine-based bridging ligands. J Inorg B 210(April):111158. https://doi.org/10.1016/j.jinorgbio.2020.111158
30. Protas AV, Popova EA, Mikolaichuk OV, Porozov YB, Mehtiev AR, Ott I et al (2018) Synthesis, DNA and BSA binding of Pd(II) and Pt(II) complexes featuring tetrazolylacetic acids and their esters. Inorganica Chim Acta 473(March):133–144. https://doi.org/10.1016/j.ica.2017.12.040
31. Alalawy MD, Socha BN, Patel UH, Patel RH, Bhatt BS, Dhaduk MP (2022) Qualitative and quantitative contributions of intermolecular interactions of dinuclear Ag complexes of sulfathiazole and sulfadiazine: X-ray crystallographic, Hirshfeld surface analysis, DFT studies and biological activities. J Mol Struct 1255:132426. https://doi.org/10.1016/j.molstruc.2022.132426
32. Varma RR, Pandya JG, Vaidya FU, Pathak C, Dabhi RA, Dhaduk MP et al (2021) DNA interaction, anticancer, antibacterial, ROS and lipid peroxidation studies of quinoxaline based organometallic Re(I) carbonyls. J Mol Struct 1240:130529. https://doi.org/10.1016/J.MOLSTRUC.2021.130529
33. Franich AA, Živković MD, Ćoćić D, Petrović B, Milovanović M, Arsenijević A et al (2019) New dinuclear palladium(II) complexes with benzodiazines as bridging ligands: interactions with CT-DNA and BSA, and cytotoxic activity. J Biol Inorg Chem 24(7):1009–1022. https://doi.org/10.1007/s00775-019-01695-w

Figures

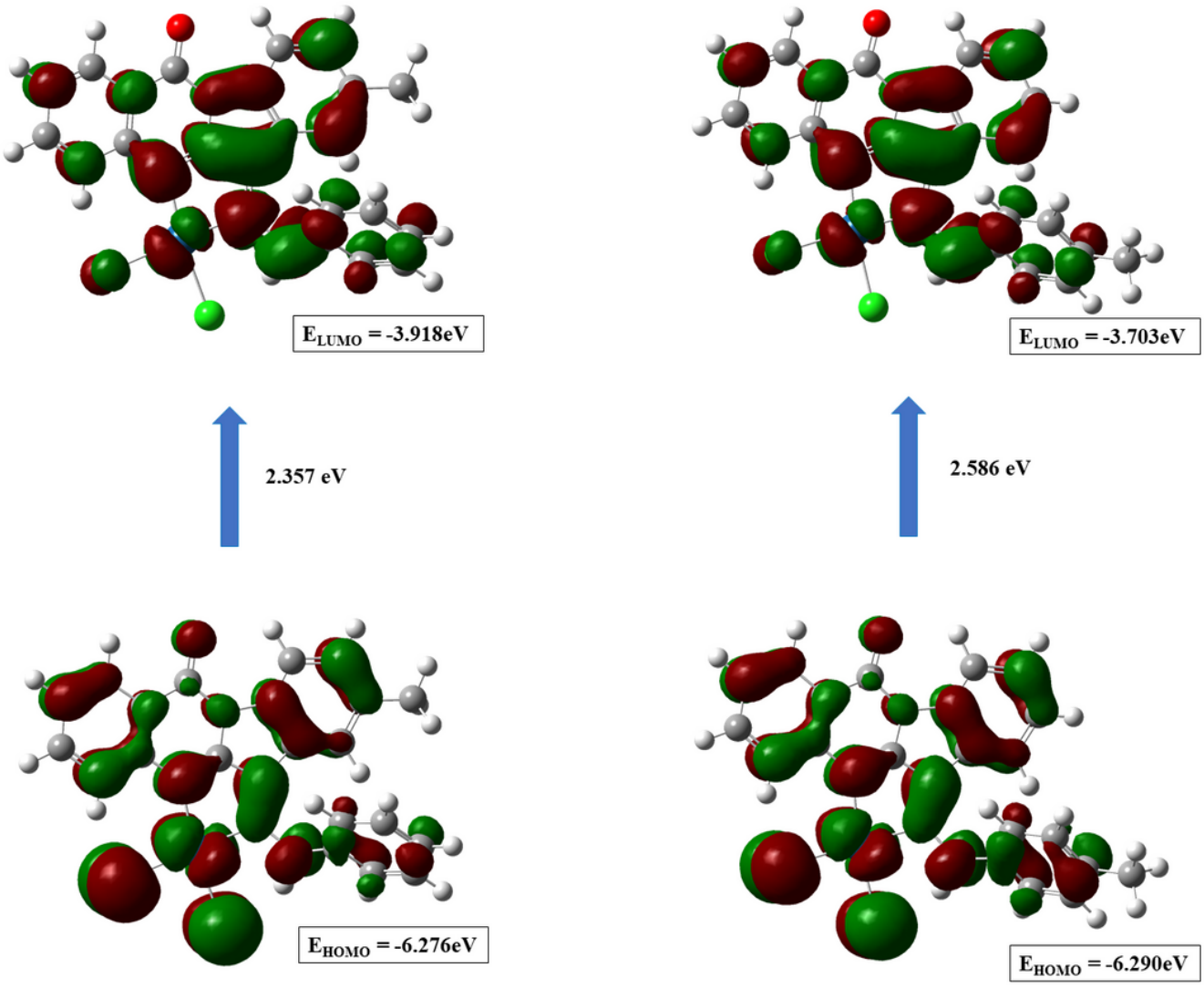

Figure 1

HOMO-LUMO energy plot of the highest(IV) and lowest(VII) energy gap.

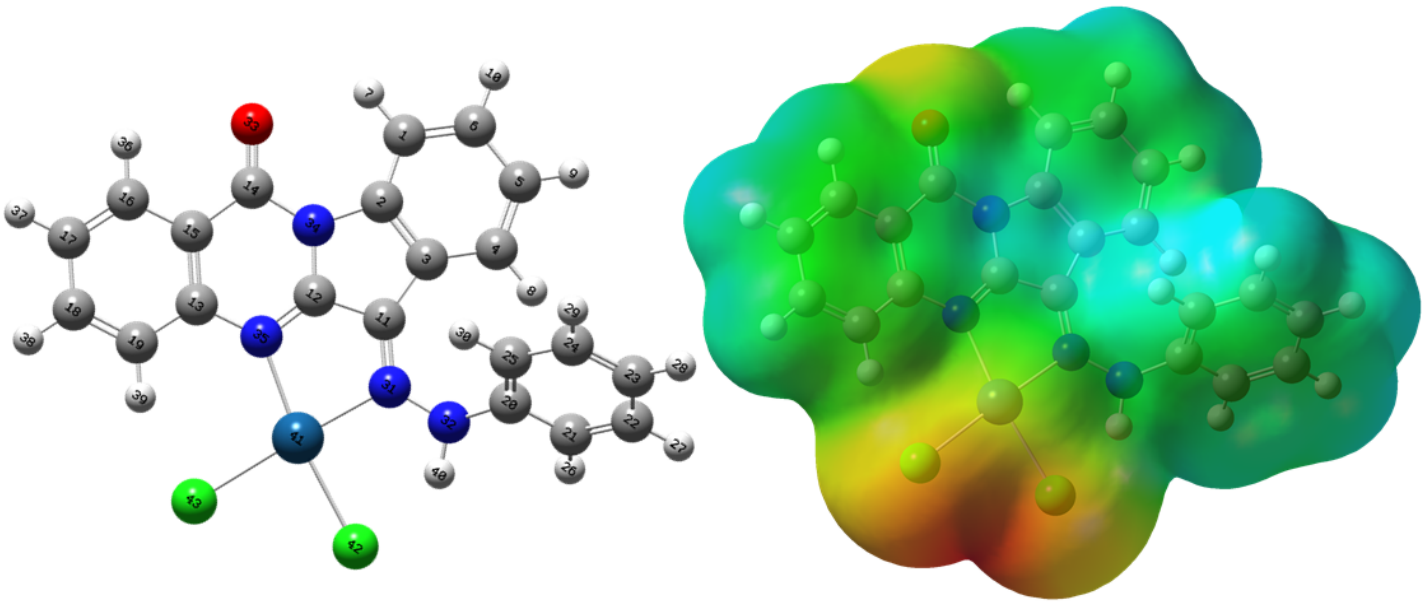

Figure 2

Optimized structure and ESP of the Pt(II) complex I

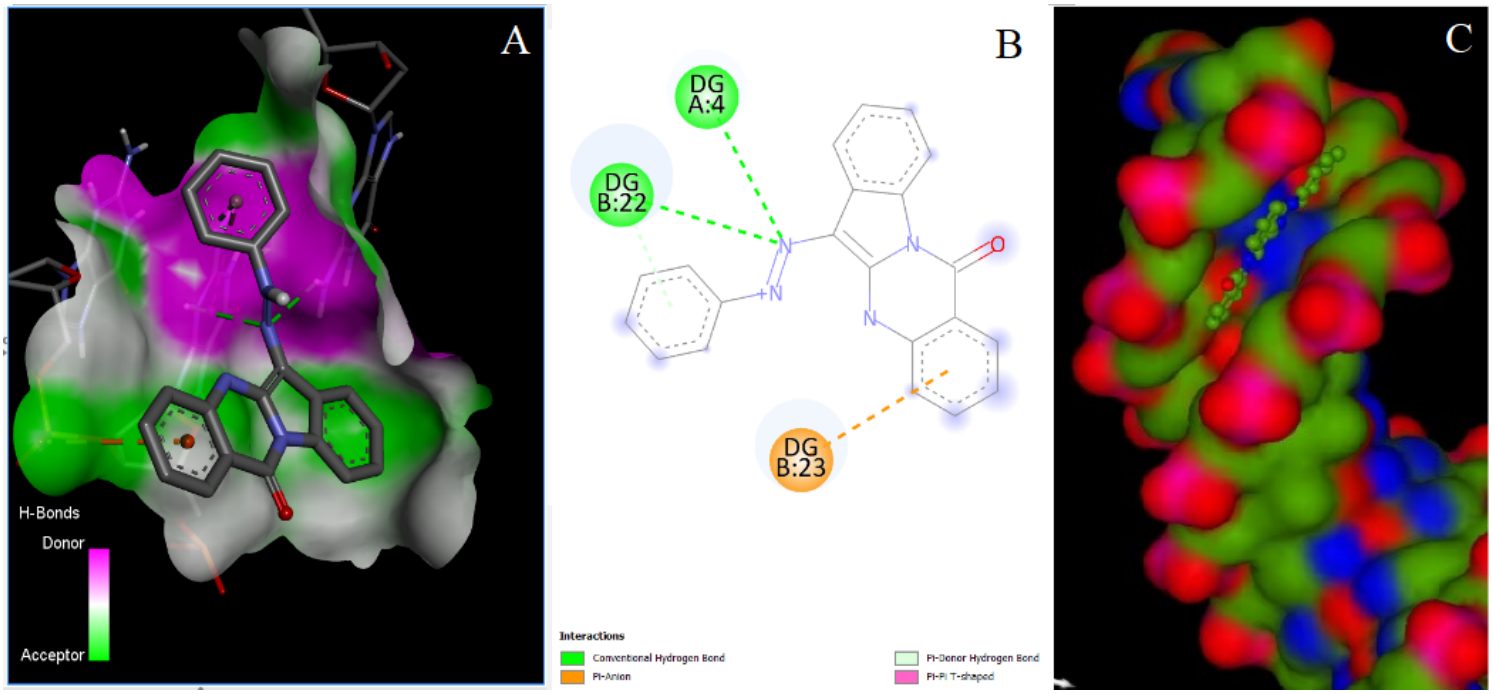

Figure 3

Docking Pause visualization of L^1

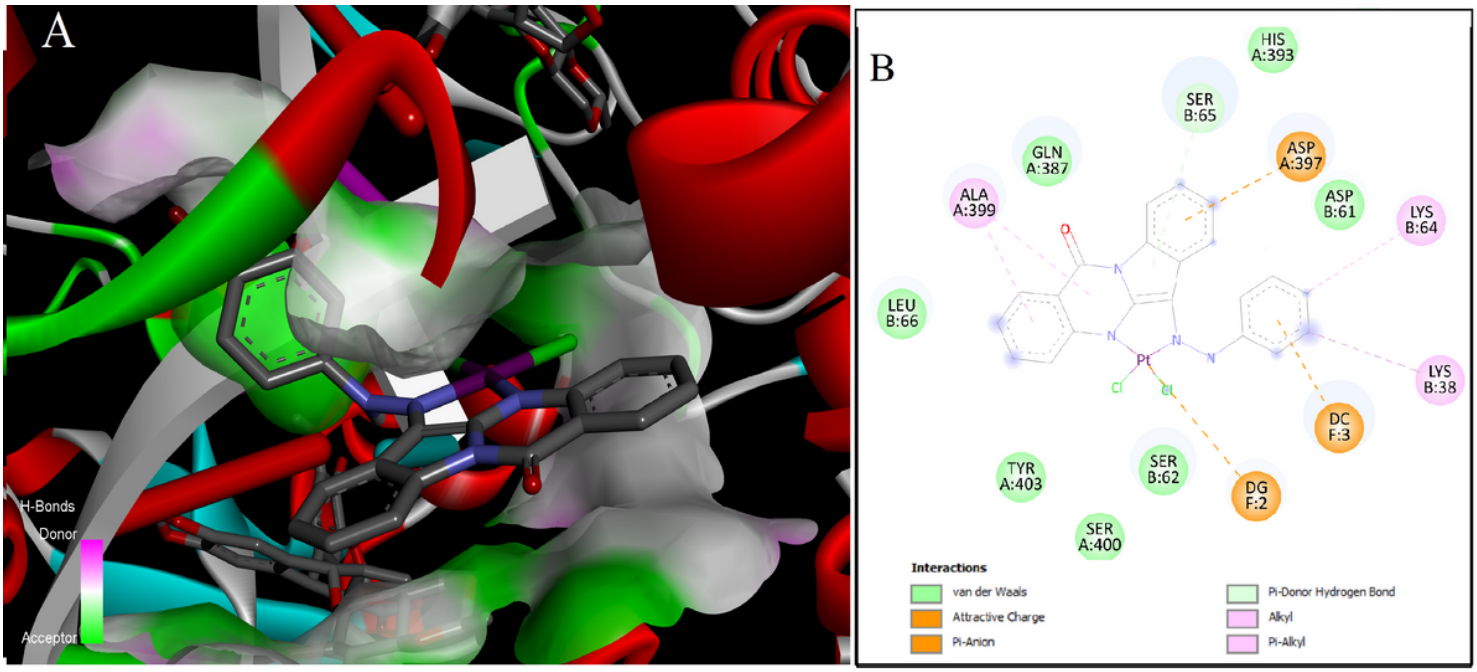

Figure 4

3D(A) and 2D(B) interaction of complex-I at the binding site.

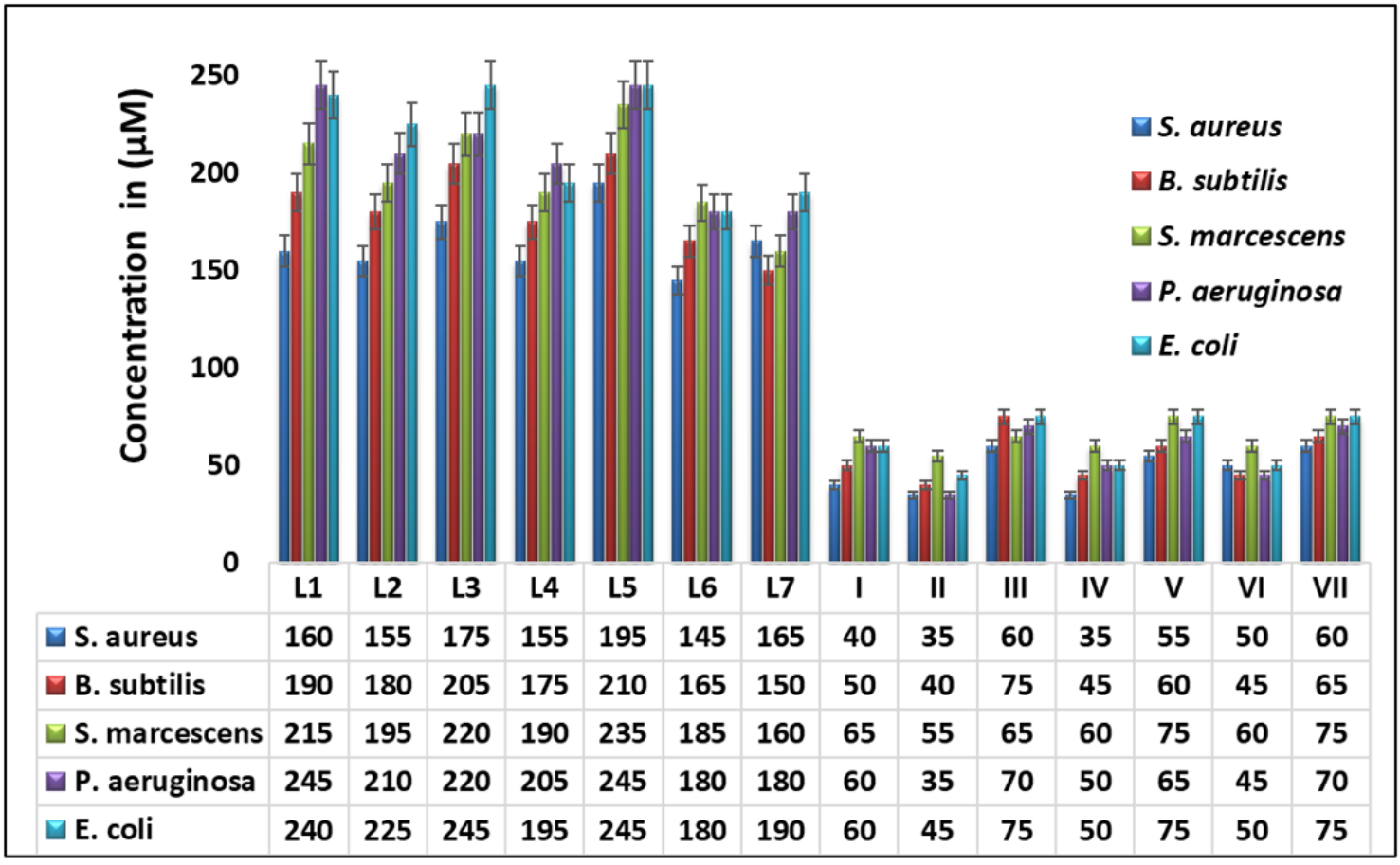

	L1	L2	L3	L4	L5	L6	L7	I	II	III	IV	V	VI	VII
S. aureus	160	155	175	155	195	145	165	40	35	60	35	55	50	60
B. subtilis	190	180	205	175	210	165	150	50	40	75	45	60	45	65
S. marcescens	215	195	220	190	235	185	160	65	55	65	60	75	60	75
P. aeruginosa	245	210	220	205	245	180	180	60	35	70	50	65	45	70
E. coli	240	225	245	195	245	180	190	60	45	75	50	75	50	75

Figure 5

Bar plot of the MIC value of the compounds

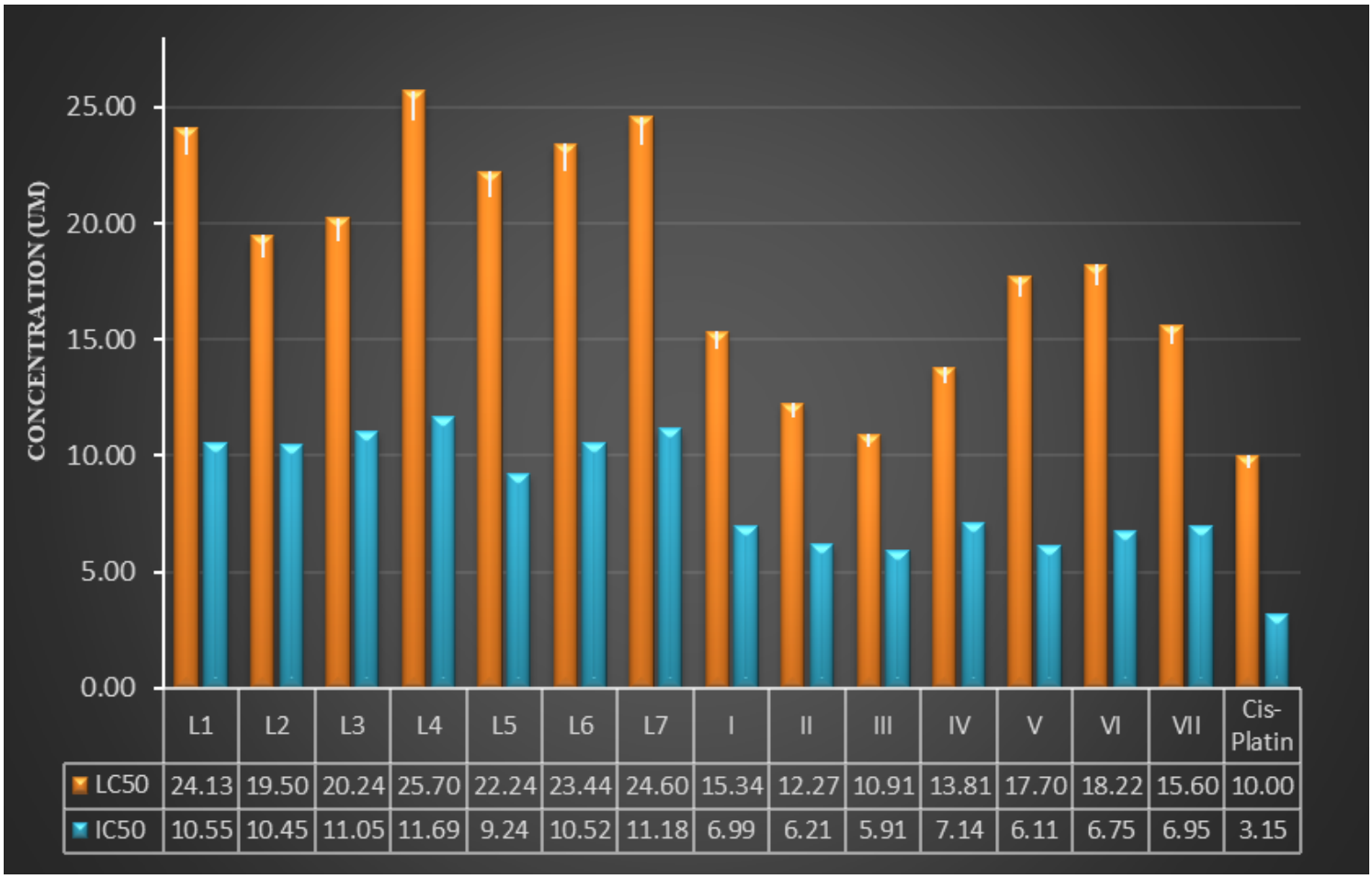

Figure 6

Bar plot of the LC_{50} and IC_{50} value of compounds

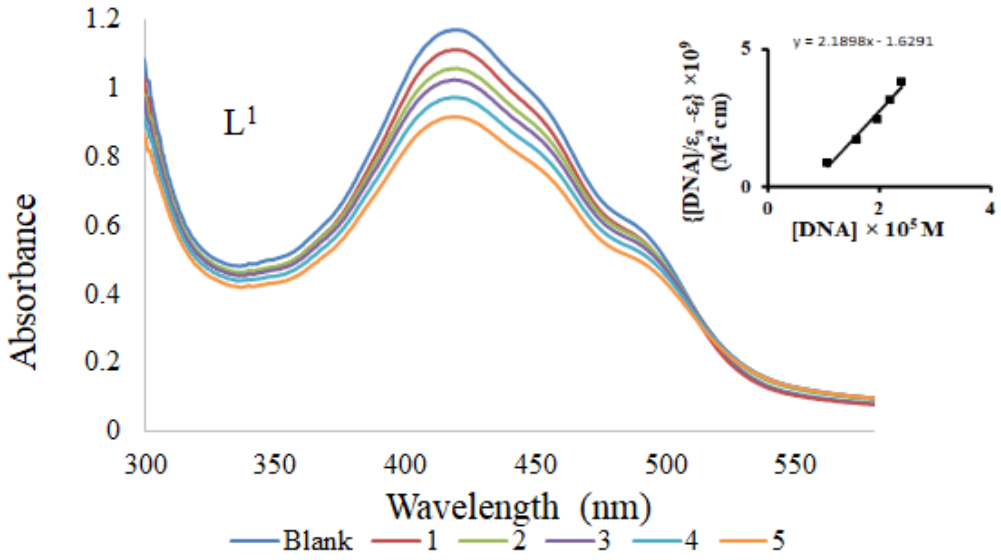

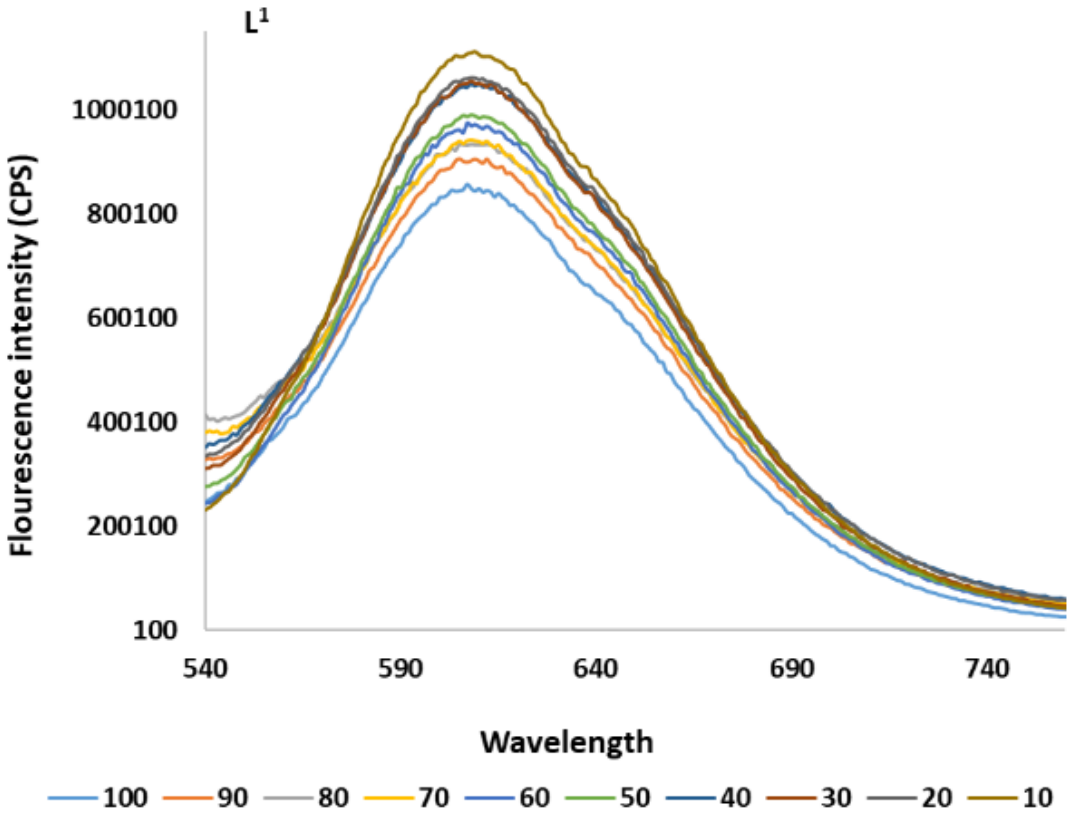

Figure 7

DNA absorption titration curve(A) DNA fluorescence titration curve(B) of Ligand 1.

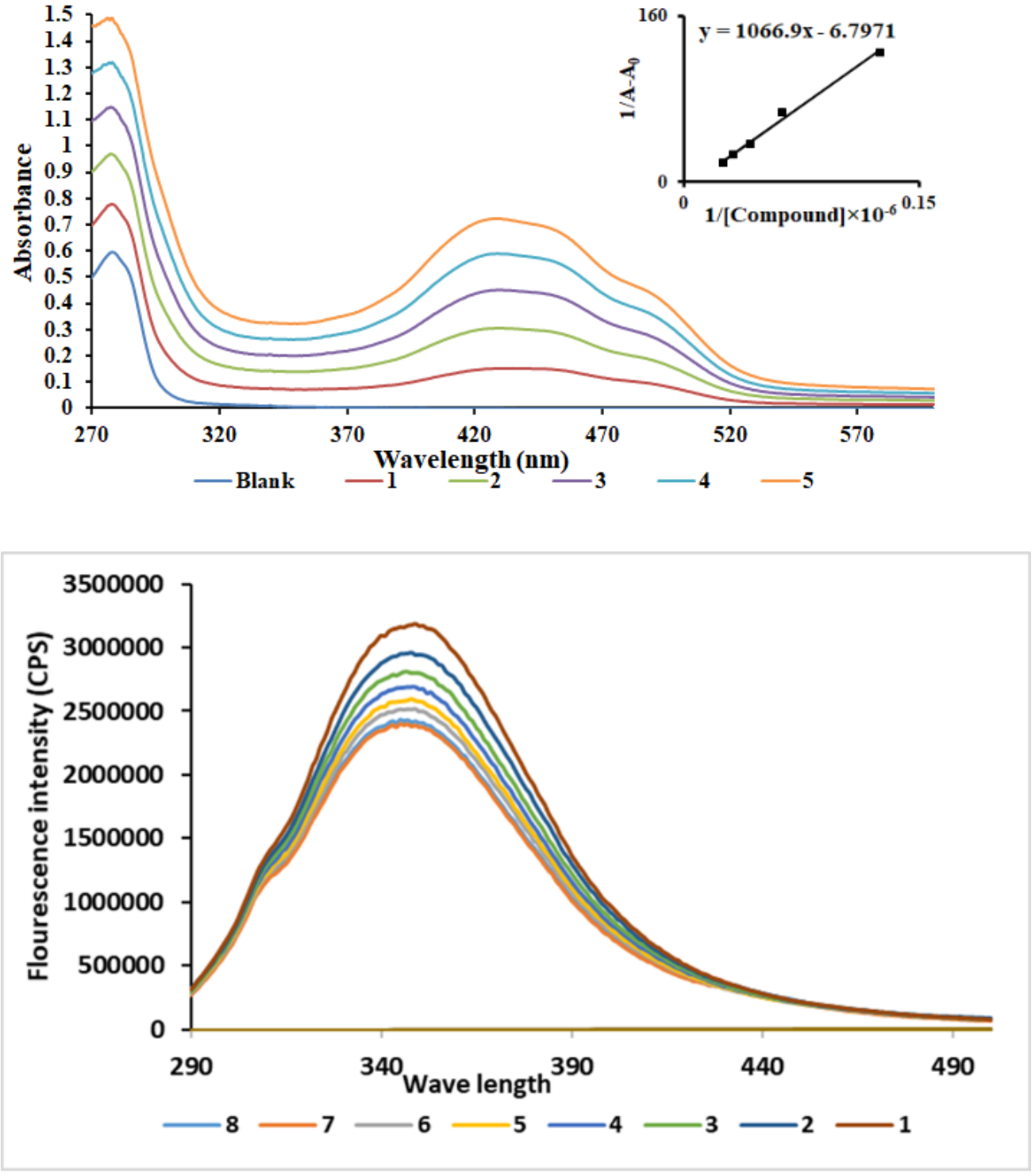

Figure 8

BSA absorption titration curve(A) BSA fluorescence titration curve(B) of complex-I.

Supplementary Files

This is a list of supplementary files associated with this preprint. Click to download.

- ElectronicSupplymentryInformation.docx